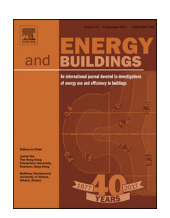
ELSEVIER

Contents lists available at ScienceDirect

Energy & Buildings

journal homepage: www.elsevier.com/locate/enbuild



Non-intrusive interpretation of human thermal comfort through analysis of facial infrared thermography



Da Li, Carol C. Menassa*, Vineet R. Kamat

Department of Civil and Environmental Engineering, University of Michigan, United States

ARTICLE INFO

Article history: Received 24 March 2018 Revised 9 July 2018 Accepted 11 July 2018 Available online 27 July 2018

Keywords: Infrared thermography Thermal comfort assessment Physiological measurements Skin temperature Non-intrusive data collection

ABSTRACT

Understanding occupants' thermal sensation and comfort is essential to defining the operational settings for Heating, Ventilation and Air Conditioning (HVAC) systems in buildings. Due to the continuous impact of human and environmental factors, occupants' thermal sensation and comfort level can change over time. Thus, to dynamically control the environment, thermal comfort should be monitored in real time. This paper presents a novel non-intrusive infrared thermography framework to estimate an occupant's thermal comfort level by measuring skin temperature collected from different facial regions using low-cost thermal cameras. Unlike existing methods that rely on placing sensors directly on humans for skin temperature measurement, the proposed framework is able to detect the presence of occupants, extract facial regions, measure skin temperature features, and interpret thermal comfort conditions with minimal interruption of the building occupants. The method is validated by collecting thermal comfort data from a total of twelve subjects under cooling, heating and steady-state experiments. The results demonstrate that ears, nose and cheeks are most indicative of thermal comfort and the proposed framework can be used to assess occupants' thermal comfort with an average accuracy of 85%.

© 2018 Elsevier B.V. All rights reserved.

1. INTRODUCTION

In the U.S. and worldwide, Heating, Ventilation and Air Conditioning (HVAC) systems represent the biggest energy end use accounting for approximately 50% of the total energy required to operate residential and commercial buildings [[16],[18]]. Despite the significant energy footprint of the HVAC systems, occupants in the built environment are often dissatisfied with their thermal comfort [[23],[31]]. For example, a large-scale survey involving 52,980 occupants in 351 office buildings suggested that only 38% of respondents are satisfied (i.e., voted "slightly satisfied" to "very satisfied") with the thermal comfort in their workplace [31].

Thermal comfort is defined as "the condition of mind which expresses satisfaction with the thermal environment and is assessed by subjective evaluation" [2]. The thermal sensation measure is affected by several human factors including physiological (e.g., gender, age), psychological (e.g., expectation, stress), and behavioral (e.g., activity level) attributes [[4],[30],[34],[39]]. As a result, thermal sensation and satisfaction have been observed to change over time in a single individual, and also vary from one person to another [26]. Even exposed to the same indoor environment, occu-

E-mail addresses: dliseren@umich.edu (D. Li), menassa@umich.edu (C.C. Menassa), vkamat@umich.edu (V.R. Kamat).

pants can still have diverse thermal sensations and preferences due to variations in their personal factors.

It is not surprising that thermal comfort has been identified as an influential factor of occupants' health and well-being [50]. For example, a high room temperature can increase the reports of sick building syndrome symptoms, such as eye, nose and throat irritation [51]. In office buildings, several studies have suggested that a satisfied thermal environment can lead to a reduced number of complaints, absenteeism, and improved working productivity [44]. However, in typical office buildings, the indoor thermal environment is usually maintained in a fixed and uniform manner. First, the thermostat is conventionally set at a consistent setpoint according to the routine practice or industry guidelines. For example, ASHRAE Standard 55 "The Environmental Conditions for Human Occupancy" recommends the comfort range as 20 °C to 24 °C in winter and 24 °C to 27 °C in summer. As a result, the HVAC system is always delivering the pre-determined amount of heating/cooling. Considering the diverse internal factors from the human perspective, such fixed industry recommendations are not satisfactory as occupants' thermal preference is evolving over time. For example, an individual entering a cool room in summer may initially feel comfortable. However, the same individual can feel cold after a while due to the continuous heat loss of human body (i.e., steady-state versus transient state sensation) [39]. Second, the current HVAC operation strategies also assume that different occu-

^{*} Corresponding author.

pants in a multi-occupancy space have the same thermal sensation and preference. This is mainly due to the lack of human data for personal comfort evaluation, as well as, the assumption that indoor environmental conditions are uniform without any spatial variations (e.g., uniformly distributed room temperature and relative humidity). Therefore, the widely adopted human-decoupled HVAC control strategy is rarely able to reach the goal of providing satisfaction to 80% of occupants [31].

In order to overcome these limitations, building HVAC systems must dynamically consider each occupant's unique thermal requirement in the control process. To achieve this goal, it is particularly important that occupants' thermal sensation and preference are interpreted and analyzed on a timely basis, if not in realtime. To this end, prior studies have established methods that require direct thermal comfort feedback from the occupants (e.g., [17],[42]), as well as, the use of intrusive data collection methods (e.g., [11],[24],[34]] and [35]) to understand the thermal condition.

Therefore, the objective of this paper is to explore the feasibility of using infrared thermography as a truly non-intrusive method to interpret human thermal comfort in indoor environments. Specifically, the authors adopted thermal preference ("warmer", "cooler", "neutral") as the target variable because it indicates the preferred comfort state of an occupant [[31],[33]]. As opposed to the existing studies which used expensive commodity cameras that need to be placed at a fixed distance from the user (detailed in Section 2.3), this study investigates an automated and real-time approach to non-intrusively obtain, retrieve, and analyze facial skin temperature features for each building occupant in real, operational indoor environments using low-cost infrared thermal cameras, computer vision and machine learning techniques.

The paper is organized to first provide a detailed review of existing research studies on the personalized control of HVAC system and thermal comfort interpretation using human data, followed by the discussion of main limitations of these studies and the contributions of our work to this body of knowledge. Then the methods for skin temperature feature extraction and data collection experiments are explained in detail in the methodology section. Finally, the comfort prediction models and the research findings are presented in the results and discussion section.

2. Background

In this section, the authors will present a review of relevant literature about methods that have been historically used for thermal comfort assessment in the HVAC controlled environments. First, the classic Predicted Mean Vote (PMV) and Predicted Percentage of Dissatisfied (PPD) models were reviewed. Second, the authors evaluated the "human-in-the-loop" approach which interprets occupants' thermal sensation and preference by requesting human feedback of the ambient environment. Third, the authors discussed the selected studies which predict an individual's thermal comfort level using personal bio-signals. The limitations of each study were analyzed to identify the research gaps in existing methods for evaluating thermal comfort in real operational indoor environment, which lead to the objectives of the proposed framework discussed at the end of this section.

2.1. PMV and PPD models

The PMV and PPD models are the most widely used methods to evaluate the indoor thermal comfort [19]. The PMV model was developed based on the thermal balance equation of human body. Four environment factors (i.e., air temperature, mean radiant temperature, air velocity, and relative humidity) and two human factors (metabolic rate and clothing insulation) are identified for thermal comfort assessment. The PMV model predicts the mean ther-

mal comfort level of a large group of people using a seven-point thermal sensation scale (from -3 for cold to 3 for hot). A thermally acceptable indoor environment is defined to maintain the PMV index within the range between -0.5 and 0.5. The PPD index is associated with the PMV index and it predicts the percentage of occupants that are dissatisfied with the thermal conditions at any given time. ASHRAE Standards 55 recommends maintaining the PPD index at less than 10%.

Despite the PMV and PPD models have been intensively used in the field of thermal comfort assessment, this method suffers from several limitations. First, the PMV model is developed based on the mean feedback of a large group of people in laboratory settings. This generalization can have a strong bias towards certain occupants in a given office environment. For example, an occupant who prefers cold environments may be treated as an outlier. Also, the PMV model assumes the same parameters (e.g., metabolic rate) for all occupants in the same space, which is unable to provide a personalized comfort prediction [32]. Second, the PMV model is originally developed for the steady-state sensations in mechanically conditioned spaces. The predictions may not hold under the transient-state conditions [[14],[52]]. In addition, occupants can perform various adaptive behaviors, e.g., opening windows or putting on an extra layer of cloth, to maintain or restore the thermally comfortable state. These adaptive behaviors can result in a wider comfort range than predictions of the PMV model [[13],[14],[45]]. Third, expensive devices are required to measure parameters such as the mean radiant temperature and metabolic rate in the PMV model, which makes it not suitable to be applied in real operational settings.

2.2. Participation-oriented thermal comfort assessment

To understand occupants' requirement of thermal environment, recent studies on personalized HVAC control have extensively investigated the "human-in-the-loop" approach which brings occupants' actual thermal sensations (also known as thermal vote) into the HVAC control loop [[17],[20],[25],[28],[33],[42]]. This control approach is initiated by thermal votes received from building occupants using a phone or web application. In each cycle, decision algorithms calculate the comfortable setpoint based on the environmental conditions and the actual thermal votes collected during this period.

For example, Feldmeier and Paradiso [20] collected occupants' thermal votes (hot, cold and neutral) together with the ambient temperature and humidity from a wrist-worn sensor to model one's thermal comfort state under various environment conditions. Jazizadeh et al. [28] used a phone application to collect thermal preferences and developed fuzzy predictive models to interpret an individual's comfort level under different room temperatures. Other studies such as Erickson and Cerpa [17] and Purdon et al. [42] adopted the similar approach which used occupants' actual thermal votes from phone applications and environment data from commodity sensors to either directly adjust the HVAC settings or model the comfort state using different statistical methods. In a recent study, Kim et al. [33] developed a personal comfort chair which can record occupants' heating/cooling requests over time. Using personal comfort models, this study achieved a 73% accuracy in predicting three-point thermal preferences (i.e., warmer, no change, cooler), which significantly outperformed the PMV and adaptive models.

Although this direct occupant participation-oriented approach provides a feasible way to understand occupants' thermal comfort in the HVAC control loop, there exist three significant limitations. First, these aforementioned studies failed to consider the influential human physiological or behavioral factors when interpreting occupants' thermal comfort. As a result, these methods may fail to

predict thermal comfort in certain scenarios due to lack of knowledge of what the human factors are under certain scenarios. For example, the same individual with different workload can have direct opposite thermal sensations and preferences in the same environment. In this case, a direct mapping from the measured environment conditions to a certain thermal comfort level is incapable of producing a robust prediction, not to mention that human factors are changing over time.

Second, in these studies, human body is assumed as a passive recipient of thermal stimuli. Several field studies suggested that occupants' adaptive behaviors (e.g., wearing a jacket when feeling cold) can play an important role in determining thermal comfort. However, this behavioral adaptation is not considered in the current voting methods. Developing a capability to capture the effects of this behavioral adaptation can result in a more flexible comfortable temperature [14].

Third and most importantly, this action-required approach heavily relies on continuous human feedback to understand occupants' comfort state over time. This is based on the assumption that the human body is the best "comfort sensor" of the thermal environment which can periodically, if not always, indicate the need to adjust temperature setpoint through feedback (i.e., requests to make the room warmer or cooler). In this case, human feedback is either used as the ground truth to rectify the comfort prediction or to directly determine the new temperature setpoint. In real life circumstances, however, this assumption is far from expected as (1) the frequency of feedback tends to decrease with time as the novelty and excitement of the system fades away [34]; and (2) the requirement of human effort in the feedback can be distracting during regular work time (especially over heavy workload periods or in any frustrating situations) and sometimes occupants are unable to vote due to a variety of reasons (e.g., the phone is not at hand).

2.3. Bio-signal oriented thermal comfort assessment

Human physiological responses (e.g., vasodilation, increased respiration) have been shown to be correlated with thermal sensations and discomfort [[29],[39]]. Therefore, detecting these human physiological responses provides a way for researchers to understand people's thermal comfort level under different conditions. This idea is implemented by measuring the variations of human bio-signals such as skin temperature, heart rate, and respiration rate. The benefits of applying bio-signals in the thermal comfort assessment are twofold: (1) bio-signals collected from each occupant allow the researchers to develop personalized comfort models, which can improve the prediction accuracy [[32],[35],[36]]; (2) bio-signals contain useful information to interpret comfort conditions and thus reduce the dependence on human participation.

Among these bio-signals, skin temperature has been intensively investigated in prior studies. The human body maintains its core temperature at around 37 °C through the thermoregulatory control of blood flow to the skin surface. During heat stress, vasodilation increases the flow of blood to the skin surface to dissipate excess internal heat, and vice versa, vasoconstriction decreases the blood flow to limit heat loss during cold stress [9]. As skin temperature is directly affected by the changes in blood flow, it is often used to estimate human thermal sensation and comfort. In practice, skin temperature can be measured using thermocouples [[10–12],[53]], infrared thermometers [24], and commodity infrared thermal cameras [[1],[5],[6],[15],[37],[43]]. Table 1 lists the device accuracy and cost in the selected studies.

Contact thermocouples are the most widely adopted devices to measure skin temperature due to their high accuracy, low-cost, and easy installation. To interpret thermal sensation and discomfort, existing studies usually attach the thermocouples to a certain body region or multiple body locations and correlate the measured temperature data under different environment settings with the local or overall thermal sensation. For example, Yao et al. [53] collected the skin temperature of different body regions from 16 copperconstantan thermocouples directly attached to the human subject. This study suggested a close relationship between the thermal sensation/comfort and the local skin temperature and developed a linear regression model to predict comfort level. Similarly, Choi and Loftness [12] measured skin temperature of multiple body parts using contact thermometers at different room temperatures, clothing and activity conditions in a climate chamber. The results showed that the gradients of temperature on hand, wrist and upper arm are good indicators to predict thermal sensation. However, this data collection method is very intrusive as the electrodes of the thermocouple should be directly attached to the skin surface. This drawback limits this approach to be feasible only in the laboratory settings as it is not possible to equip each occupant with the thermocouples in the operational residential or office environment without interfering with their activities.

An infrared thermometer is a low-cost temperature sensor that can provide a non-contact measurement of skin temperature. However, in order to get an acceptable skin temperature measurement, infrared thermometers need to be placed close to the skin surface usually within a few centimeters. This is due to the fact that its field-of-view (FOV) becomes increasingly large as it moves away from the target. For example, Ghahramani [24] installed four MLX90614 infrared thermometers on an eyeglass frame to collect a user's skin temperature of the front face, cheekbone, nose and ear. The infrared thermometer adopted in this study has a FOV of 90° and thus for every 1 cm away from the object, the sensing area grows by 2 cm [46], which makes the eyeglass frame an ideal (and possibly the only feasible) location to place the sensors. This study observed significant variations in skin temperature under cold and heat stresses. However, this approach has two major limitations: (1) due to its limited working range, infrared thermometers can only measure a fixed predetermined set of locations. It is unknown whether these selected sensing points are the most significant locations to measure skin temperature; and more importantly (2) this approach is not suitable in a real operational or multi-occupancy environment as it requires each occupant to wear such devices, which can be inconvenient and lacks scalability in a large space with multiple occupants such as a lounge or a conference room.

Using thermographic cameras (also known as thermal cameras) is an alternative way to collect skin temperature data without contacting the object. Thermal cameras have a longer and a more flexible working range but usually suffer from a relatively lower accuracy compared to the thermocouples and infrared thermometers. However, they are able to provide a full image frame of thermographic measurements from which the users can get the temperature reading at each pixel location. Prior studies such as Abouelenien et al. [1], Burzo et al. [[5],[6]], De Oliveira et al. [15], Ranjan and Scott [43] have used commodity thermal cameras to collect skin temperature and correlated it with thermal sensations using different statistical methods. A recent study by Metzmacher et al. [37] used Microsoft Kinect and a dynamically calibrated commodity thermal camera to track human faces and measure skin temperature of different facial regions. The temperature measurements from the thermal camera were validated using a reference sensor which was attached to the skin.

In addition, three significant limitations of these aforementioned studies should be acknowledged: (1) thermal camera is used as an independent tool to measure human skin temperature which is then analyzed offline in a disconnected way, rather than a built-in component of the building automation system (BAS) or HVAC system which can dynamically monitor the indoor ther-

 Table 1

 Comparison of skin temperature measurement devices in different studies.

Studies	Device	Accuracy	Cost
[10]	Corte DermaLab System*>	±0.2 °C	~\$1,200
[11]	STS-BTA Surface temperature sensor*	$\pm 0.2~^{\circ}\text{C}$ at $0~^{\circ}\text{C}$, $\pm 0.5~^{\circ}\text{C}$ at $100~^{\circ}\text{C}$	\sim \$250 (including the hub)
[24]	MLX90614 infrared thermometer*	±0.5 °C	\sim \$150 (including the Arduino)
[5,6]	FLIR Thermovision A40	± 2 °C or $\pm 2\%$ of Reading	~\$6,000
[43]	FLIR A655sc thermographic camera	± 2 °C or $\pm 2\%$ of Reading	~\$22,000
[1]	FLIR SC6700 thermal camera	± 2 °C or $\pm 2\%$ of Reading	~\$15,000
[37]	FLIR A35 thermographic camera	± 5 °C or $\pm 5\%$ of Reading	~\$5,000
This study	FLIR Lepton 2.5	±5 °C or ± 5% of Reading	~\$200 for camera

^{*} denotes the intrusive data collection method.

mal environment; (2) as these works are more exploratory studies, thermal cameras are required to be placed directly in front of the subject, usually within a fixed distance. Again, this significantly limits the applicability of thermal cameras in the real operational settings as occupants can move around at will; and (3) the commodity thermal cameras are cost prohibitive (in excess of \$5000, see Table 1) and not suitable for large scale applications. It is still unknown whether low-cost thermal cameras (at the cost of accuracy) can be used for thermal comfort assessment which is what this paper aims to investigate.

Prior work by the authors [[34],[35]] investigated personalized thermal comfort prediction using integrated human and environment data collected from multiple sources including wristbands, polling apps, and commodity sensors. The results from these studies indicated that quantitative human data (such as skin temperature, heart rate) can significantly improve the accuracy of thermal comfort prediction. However, this approach still suffers the problem in terms of intrusiveness as occupants are required to wear the wristband and use the phone app.

To overcome the research gaps identified in the existing body of knowledge, it is critical to explore a truly non-intrusive and scalable framework which can predict human thermal comfort preferences in various settings in real time. Thanks to the current advancements in infrared thermography, low-cost thermal cameras are available in the market and offer an ideal approach due to their capability to non-intrusively capture infrared signals emitted from the human body, their affordable price and compact size, ease of installation, and preservation of occupants' privacy. To this end, this paper investigates an automated and scalable framework to non-intrusively obtain, retrieve, and analyze skin temperature data to achieve a robust thermal comfort assessment for each building occupant in a real building environment using infrared thermal cameras and computer vision techniques.

3. Methodology

This study leverages a range of techniques to develop an integrated framework for comfort assessment using low-cost/off-theshelf thermal cameras. These techniques include (1) computer vision (e.g., Haar cascade object detection) to detect human face and extract region of interest (ROI); (2) statistical methods to clean and analyze the raw skin temperature data (e.g., Kernel smoother); and (3) machine learning methods to develop personalized comfort prediction models and analyze significant facial skin temperature features (e.g., Random Forest classifier). An overview of the operating principle of the proposed non-intrusive thermal comfort assessment framework is shown in Fig. 1. In this framework, facial skin temperature is selected as the targeted bio-signal. This is because the human face has a higher density of blood vessels than other skin surfaces, leading to a larger skin temperature variation when the condition of human body or ambient environment changes [48]. As a result, facial skin temperature can be used as a physiological indicator of an individual's overall thermal comfort

Table 2 Specifications of FLIR Lepton 2.5.

Features	Descriptions
Dimensions Resolution Thermal sensitivity Accuracy Price	$8.5\times11.7\times5.6$ mm $80(h)$ x $60(v)$ pixels <50 mK ±5 °C or $\pm5\%$ of reading in the working range \$199

[[24],[54]]. Second, human faces are not covered by clothing and thus the emitted infrared energy can be directly measured by the thermal camera. In addition, human faces allow the computer vision algorithms to detect and locate ROI in the image frame for data analysis.

The remaining methodology section was organized to first introduce the sensors and devices adopted in this study. Second, the authors discussed how computer vision is applied to extract skin temperature of the ROI. Finally, the data collection experiment was explained in detail.

3.1. Low-cost thermal camera

In this study, the FLIR Lepton 2.5 radiometric thermal camera core was used to collect skin temperature data (see Fig. 2). FLIR Lepton 2.5 is an uncooled long-wave infrared thermal imaging core with a factory-calibrated temperature value. Relevant specifications can be found in Table 2 [21].

As a low-cost thermal camera, the radiometric accuracy of Lepton 2.5 is relatively low in its full operational temperature range (-10 °C to 65 °C) compared to the advanced models or thermocouples. However, its feasibility is still worth investigation due to four reasons: (1) the nominal accuracy in Table 2 ($\pm 5\%$ of reading) can be overestimated as the measuring objects in this study are human faces whose surface temperatures are not high (approximately 35 °C); (2) the room temperature of the experiment is set between 22 °C and 28 °C rather than the camera's full operational temperature range. As a result, the impact of environmental temperature variations on the measurement accuracy should be low [21]; (3) continuous thermal videos rather than a single image frame are used to interpret thermal comfort. The random measurement errors can follow a Gaussian distribution and thus it is possible to reduce the error to an acceptable level for thermal comfort interpretation by removing outliers and averaging multiple image frames; (4) the objective in this study is to predict a 3-point thermal preference, i.e., warmer, neutral, and cooler. This is considered a classification problem, rather than a regression problem which calculates a seven-point scale thermal sensation (e.g., [55]). Therefore, the problem setting is more robust to the error of measurements. For example, an error of 0.5 °C might lead to a prediction error between slightly warm and warm sensations; however, this error is acceptable since both are categorized into "preferring a cooler environment". In addition, the three-point preference pre-

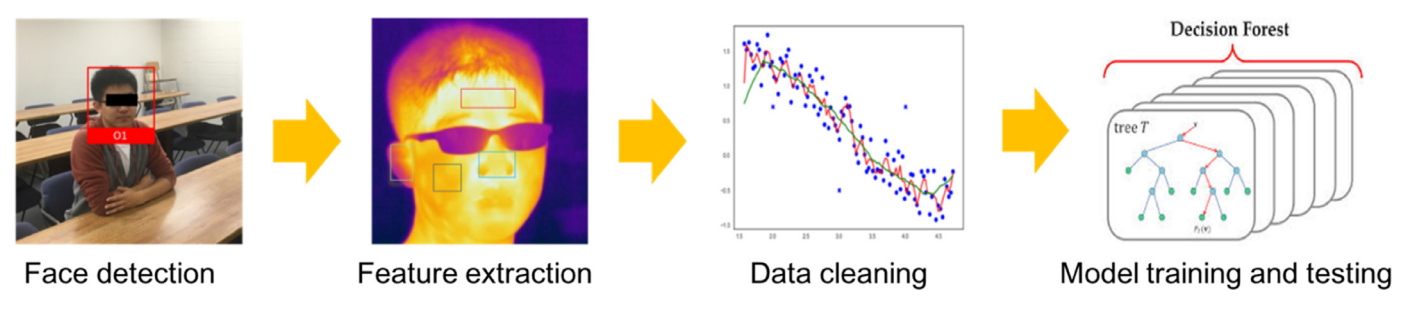


Fig 1. Overview of the non-intrusive thermal comfort interpretation framework.

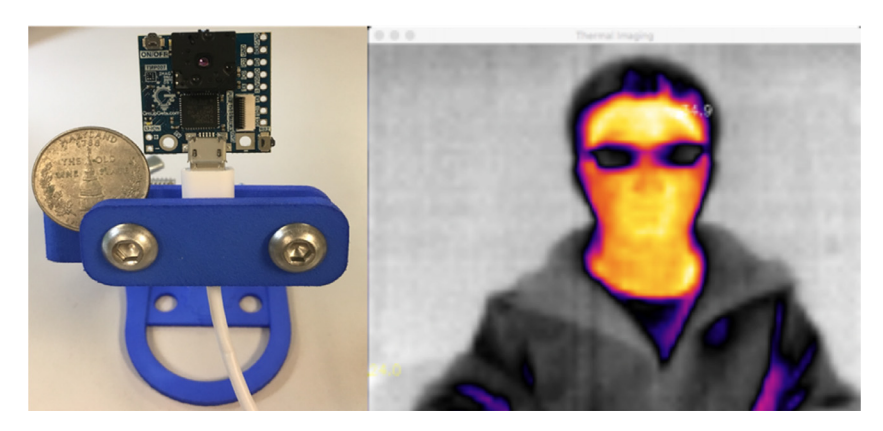


Fig. 2. FLIR lepton 2.5 radiometric thermal camera core (left) and thermal image (right).

diction should not be considered as a limitation as the control system can dynamically determine whether to increase or decrease the setpoint by continuously predicting one's preferences, which can lead to a better thermal environment.

In order to evaluate the measurements from the low-cost Lepton 2.5, the authors conducted a comparative preliminary experiment using a FLIR T450SC thermal camera (accuracy $\pm\,1\,^{\circ}\text{C}$ or $\pm\,1\%$ of reading, approximate cost is in excess of \$10,000). Facial skin temperature measurements from these two cameras (i.e., FLIR Lepton 2.5 and FLIR T450SC) were compared to confirm the feasibility of the proposed approach before conducting the following data collection experiments. Details about the comparative validation can be found in Section 3.2.2.

3.2. Face detection and skin temperature feature extraction

To extract skin temperature features, the contour of human faces and the interested facial regions are first detected in each thermal image frame. The temperature measurements of each identified region are then extracted and processed to produce the skin temperature features, which are validated in the comparative study.

3.2.1. Face detection from the thermal image

Although Lepton 2.5 has a lower resolution (80 by 60), the outline of the interested regions (e.g., forehead, nose, cheeks) are clearly preserved in the thermal image (see Fig. 2, which was taken from 1 m away to represent a non-intrusive distance), which makes the Haar Cascade algorithm suitable for this task. Haar Cascade is a fast and effective algorithm for frontal and profile face recognition by detecting the existence of certain characteristics in the image, such as edges or changes in texture [49]. In this study, the Haar Cascade algorithm was applied to detect the existence of the facial contour, the eyes, and the nose using the OpenCV package. Other regions such as forehead, cheeks, ears, mouth, and neck were inferenced from their relative locations (facial geometry) to



Fig. 3. Detection of ROI and extraction of temperature (for demonstration purpose, each region was highlighted in a solid rectangle).

the known regions (i.e., facial contour, eyes, and nose can help identify the location of the cheeks) during the runtime. These ROIs were selected based on prior studies such as Ghahramani [24], Metzmacher et al. [37], and Yi and Choi [54]. The size and location of each inferenced ROI were tuned on several subjects prior to data collection experiments to ensure the algorithm can correctly detect all features across different subjects. The measurements of each pixel located within the identified ROI were averaged to represent the corresponding skin temperature of each facial region (as shown in Fig. 3). In each ROI, pixel values exceeded certain thresholds (e.g., below 28 °C or above 38 °C based on the preliminary results) were filtered out as they were likely to be the background or

noise, which can interfere with the measurements of skin temperature features. For example, a close-by light bulb might be detected in the ROIs on faces. If not removed, the resulting high measurements can lead to a wrong prediction that the subject is too warm. Using this approach, the authors extracted a total of 26 facial skin temperature features which include the maximum measurement of human face and its gradient, as well as, the maxima, minima, mean, and gradient temperature of six facial regions (i.e., forehead, nose, cheeks, ears, mouth, and neck). For the gradient temperature, the mean gradient over a five-minute period (e.g., [7]) was calculated as shown in Eqs. (1) and (2).

$$\nabla T_i = \frac{(T_c - T_{c-i})}{i}, \quad i = \{1, 2, 3, 4, 5\}$$
 (1)

$$\overline{\nabla T} = \frac{1}{5} \sum_{i=1}^{5} \nabla T_i \tag{2}$$

Where ∇T_i is the gradient temperature for time interval i; T_c is the temperature measurement at time c; $\overline{\nabla T}$ is the mean gradient temperature over five minutes which is selected as a feature.

After extracting skin temperature for the six facial regions from each frame, the thermal image is immediately discarded to alleviate the privacy concerns.

Based on the preliminary experiments, this approach can successfully perform face detection within a camera distance of 2 m, which is a reasonable non-intrusive distance as the thermal cameras can be mounted on the wall or desktop in front of the users at this distance. If the thermal cameras were placed further away from the subject, this approach may fail as the edges on the human face are blurred in the thermal images. To overcome this limitation, the authors have explored RGB camera guided feature extraction, which can achieve a robust detection of ROI from a further distance. The preliminary results were promising but beyond the scope of this paper.

3.2.2. Preliminary accuracy evaluation of the Low-cost thermal camera

As mentioned earlier in Section 3.1, in order to evaluate the accuracy of the proposed low-cost Lepton 2.5, comparative preliminary experiments were conducted in a climate chamber under three experimental conditions (i.e., cooling from 28 °C to 22 °C, heating from 22 °C to 28 °C, steady-state condition at 25 °C). Each experiment lasted for 40 minutes and a thermal image was taken by the reference FLIR T450SC camera every 5 minutes. Each ROI in the reference image was labeled using the FLIR ResearchIR software (see Fig. 4) which provides the mean measurement in each selected region (after removing the outliers). The Lepton 2.5 camera was placed at 1 m from the participant. The authors compared the reference measurements (from the FLIR T450SC) with the temperature retrieved (from Lepton 2.5) using the approach discussed in Section 3.2.1. The results showed that in most cases the differences between two cameras were within 1 °C. A few examples from the steady-state experiment were presented in Fig. 5. However, it should be noted that this comparison was a sanity test of the face detection and skin temperature extraction approach as discussed in Section 3.2.1. The temperature deviations highly depend on how each region was labeled in the ResearchIR software. For example, the forehead region in Fig. 3 is larger and contains some low temperature pixels (e.g., the eyebrows and pixels close to hairs) compared to the same region in Fig. 4, which can be a major cause of the large deviation (about 1 °C). However, the nose region in the two images look identical and the deviations can be as low as 0.2-0.3 °C, which is acceptable given this results from a low-cost camera.



Fig. 4. Reference thermal image taken by FLIR T450SC (colored boxes represent the manually labeled ROI).

3.3. Data collection experiments

For data collection, the authors designed an experiment to collect skin temperature data and the participants' corresponding thermal responses under three thermal conditions. The data collection experiment was conducted in a research office at the University of Michigan (UM) during the heating season from December 2017 to February 2018. During this period, the average high and low outdoor temperature was 1.6 °C and -6.7 °C, correspondingly.

In the testbed office, one thermal camera was placed 1 m away from the subject which monitors the frontal face (see Fig. 6). The testbed office had two COZIR temperature/humidity sensors (humidity accuracy: \pm 5%; temperature accuracy: \pm 1 °C) to continuously monitor the ambient conditions within the close proximity to the subject during the experiment. The two sensors were placed at the waist level (0.65 m above the floor) which is close to the specified height of 0.6 m for seated occupants in ASHRAE standards 55 [2]. The testbed also had a thermostat by which the research team can freely change the indoor temperature from 20 °C to 28 °C. In the experiments, the room temperature was set between 22 °C and 28 °C, which conforms to typical indoor conditions controlled by the mechanical HVAC system (ASHRAE 55).

Each subject in this study was assigned a reference ID number for data storage and analysis. The subjects were all students from UM aged between 22 and 27 and were healthy at the time of the data collection. Subjects were asked to wear a sweatshirt and pants and keep the same clothes during the experiment as outlined in Fig. 7. The experiment started by an interview to understand the subject's interpretation of thermal comfort (e.g., when you feel cold, do you focus on overall body sensation or the sensation of specific body parts?). Introductions about the devices, research objectives, and other related information have been provided to help subjects understand this study. Then, each subject completed an experiment consisting of four phases (see Fig. 7). In the preparation phase, each subject was provided with a designated phone app (see Fig. 8) which was customized for this study (more details about the phone app can be found in [35]). Subjects can vote their thermal preferences using the three-point scale (i.e., warmer, cooler, neutral) through this phone app.

During the whole data collection experiment, subjects were asked to use the phone app to provide thermal feedback every three minutes which will be used to develop and evaluate comfort prediction models. At the same time, the facial skin temperature and environment conditions were continuously monitored and uploaded to the database. In the 60-min steady-state phase, subjects

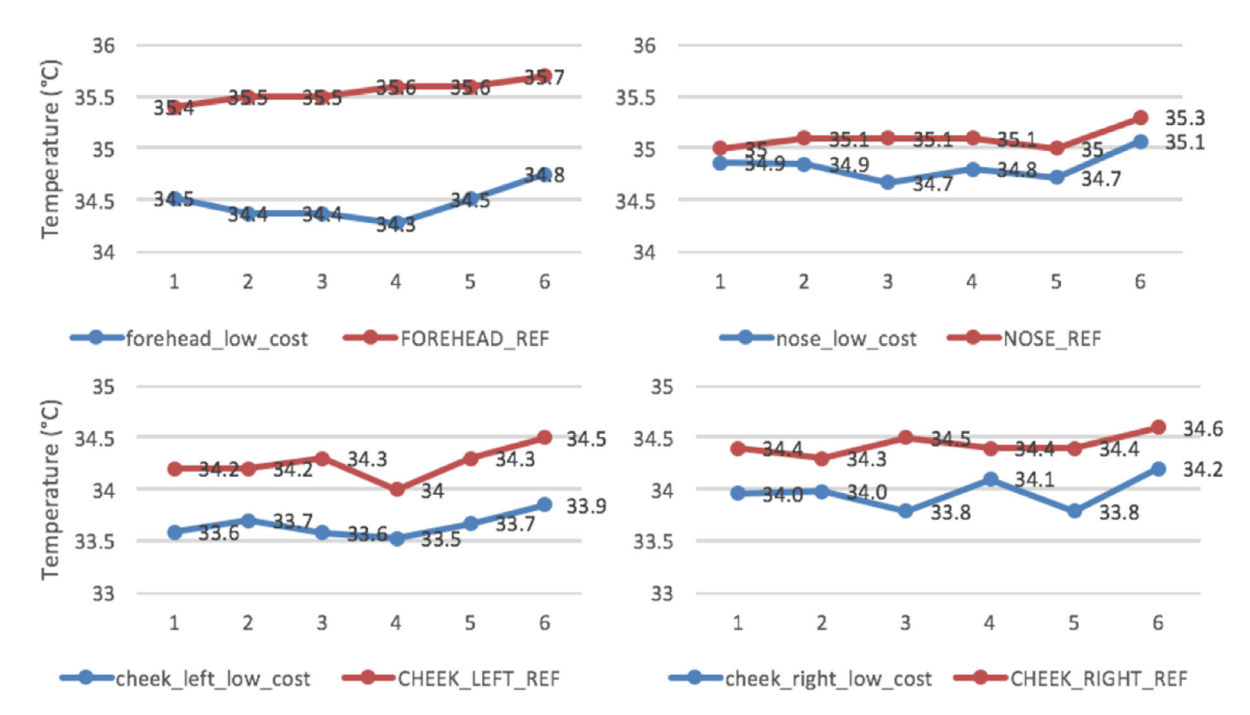


Fig. 5. Comparison of the low-cost camera with the reference camera.

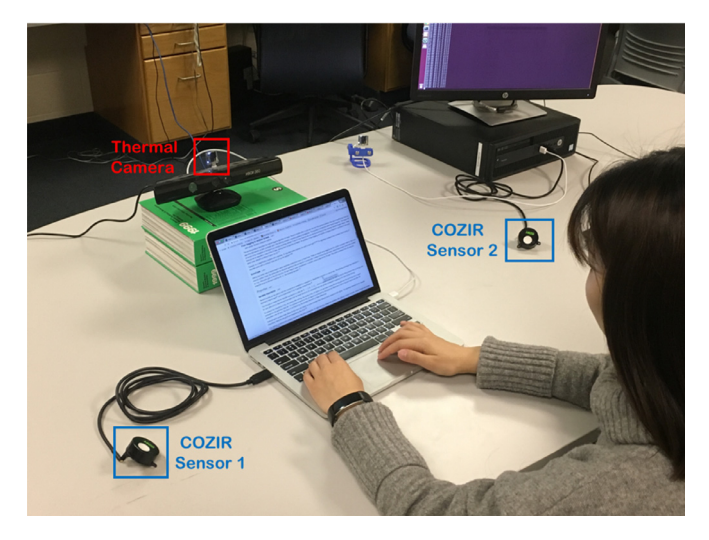


Fig. 6. Experiment setup.

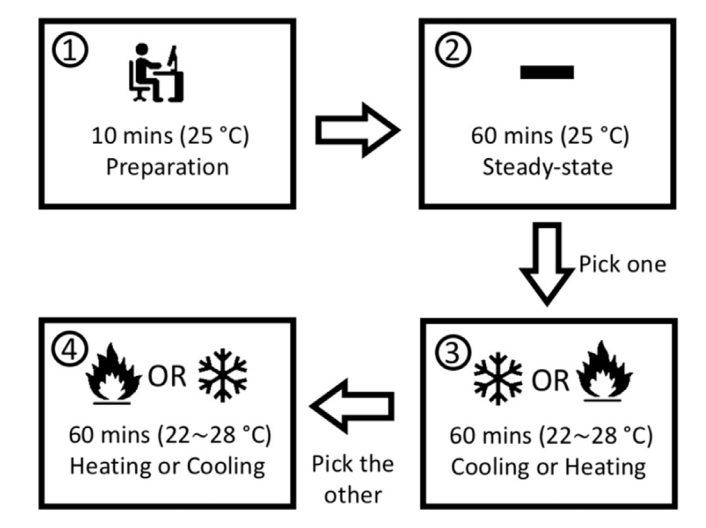


Fig. 7. Timeline of the data collection experiment.

4. F

were asked to perform daily office activities such as reading, typing, or browsing. In this phase, room temperature was maintained at 25 °C to represent a neutral steady-state condition. Next, the cold stress or heat stress phase started in a random order. In the 60-min heat stress phase, room temperature was increased from 22 °C to 28 °C while for the cold stress phase, room temperature was decreased from 28 °C to 22 °C. The two environment sensors showed that in both phases the room temperature was approximately changed in a linear manner with time (at a rate of $\pm\,1\,^{\circ}\text{C}$ per 10 minutes). It is worth noting that this random order configuration was chosen to help eliminate subjects' bias towards thermal sensation and comfort. For example, if a subject knows the current room temperature is decreasing, he/she may unconsciously think he/she is getting cold. The data collection experiment has been approved by UM Institutional Review Board (IRB) for conducting human subjects research.

4. Results

4.1. Data cleaning and smoothing

In the proposed approach, the measurement errors of skin temperature mainly came from three sources: (1) thermal camera's systematic error caused by the temporal drift which accumulates over time [21]. For example, thermal images appear blotchy due to the degrade uniformity which affects the radiometric accuracy; (2) random experiment error which may vary from one observation to another. For example, hands are detected as the mouth region when subjects drink water during the experiment which corresponds to a spike in the raw data; and (3) random measurement error of the thermal camera which is assumed to follow a Gaussian distribution with a zero mean. For the camera's systematic error, Lepton 2.5 automatically performs a flat-field correction (FFC) every three minutes to compensate for the drift effect. During FFC, the camera closes the shutter and recalibrates the sensor based on

Table 3Summary of environment conditions in three phases.

	Cooling			Heating			Steady-State		
	Range	Mean	S.D.	Range	Mean	S.D.	Range	Mean	S.D.
T (°C)	27.5 - 22.6	25.1	1.4	22.5 - 27.7	25.3	1.5	24.5 - 25.2	24.8	0.2
RH (%)	20.2 - 33.4	27.7	3.6	32.5 - 21.4	25.8	2.2	20.6 - 26.5	23.2	0.5



Fig. 8. UI for the designed app [35].

a uniform thermal scene. For the other two random errors, the authors first averaged the image frames captured in each minute and removed outliers by checking the difference of adjacent measurements using Eq. (3).

$$d_{i} = \begin{cases} outlier, & if \ d_{i} - d_{i-1} \ge 3\sigma \\ not \ an \ outlier, & otherwise \end{cases}$$
 (3)

Where d_i and d_{i-1} are the data collected at time i and i-1, and σ is the standard deviation of data collected from time 0 till time i. After removing the outliers, a Gaussian filter was applied to smooth the raw data. Different widths of the Gaussian filter have been compared (width = 5, 7 and 10). Considering the duration of the experiment, the authors chose the filter width to be 7 as it smoothed the data well and also preserved the trend of measurements. For example, Fig. 9 shows a subject's maximum skin temperature in three phases (i.e., heating, cooling, steady-state) where the dashed lines represent the raw data collected directly from the thermal camera and the thick solid lines represent the processed data after removing outliers and smoothing. Through data processing, large measurement errors are removed before applying further analysis, resulting in a smoothed curve for each experiment. In addition, it is easy to observe the increasing and decreasing trend of skin temperature in the heating and cooling phases while the measurements are relatively stable in the steady-state phase, which indicates that useful information is well preserved after the processing step.

4.2. Correlation analysis between identified regions

A total of 12 subjects (7 male, 5 female) participated in the data collection experiments as discussed in Section 3.3. The environment conditions of the three phases were summarized in Table 3. As shown in the table, room temperature in the steady-state phase was maintained at around 25 °C with a standard deviation of \pm 0.2 °C, which was close to the mean temperature of cooling and heating phases. Skin moisture level has been suggested to influence the emissivity of skin surface, which affects the accuracy of temperature measurements [22]. However, the authors did not observe obvious and excessive sweating for any subject at the high room temperature (around 28 °C), suggesting the emissivity can be assumed consistent in the experiment given the insignificant changes in skin moisture level. This is supported by the work

of Owda et al. [38] which compared the emissivity of wet skin sample (taken from a human cadaver and rinsed in water) and dry samples (dried for a 4.0 h prior to measurements). Table 4 shows a summary of skin temperature feature statistics in the three phases. The mean and standard deviation (SD) of each feature were calculated from Eqs. (4) and (5) as shown below.

$$\bar{\mu} = \frac{1}{n} \sum_{k=1}^{n} \mu_k, \quad SD(\bar{\mu}) = \sqrt{\frac{1}{n-1} \sum_{k=1}^{n} (\mu_k - \bar{\mu})}$$
 (4)

$$\bar{s} = \frac{1}{n} \sum_{k=1}^{n} s_k, \quad SD(\bar{s}) = \sqrt{\frac{1}{n-1} \sum_{k=1}^{n} (s_k - \bar{s})}$$
 (5)

Where $\bar{\mu}$ and $SD(\bar{\mu})$ are the mean and standard deviation of skin temperature of all subjects in a particular phase; \bar{s} and $SD(\bar{s})$ are the mean and standard deviation of the sample standard deviation; n is the number of subjects which is 12 in this study.

In the heating and cooling phases, subjects in general demonstrated all the three thermal preferences considered for this study at different times of the experiment. For example, in the heating phase a subject may initially prefer a warmer environment as the room temperature starts from 22 °C; gradually he/she feels thermally neutral as the room temperature increases; and finally he/she may prefer a cooler environment as the room temperature exceeds the comfortable range. However, as the room temperature is controlled at a constant level in the steady-state phase, subjects usually have the same preference throughout this phase.

As shown in Table 4, the standard deviations of the mean skin temperature range from 0.62 °C to 1.84 °C (see $SD(\bar{\mu})$ shown in bold in column 1, 3, and 5), which indicate temperature variations of each facial region between different subjects. In the cooling and heating phases, the cheek region shows the highest skin temperature variation across all subjects (cooling: SD: 1.84 °C, heating: SD: 1.66 °C) and the same for the nose region (SD: 1.54 °C) in the steady-state phase. The lowest personal variations in the three phases are observed in the neck (cooling: SD: 0.83 °C). nose region (heating: SD: 0.66 °C), and facial maxima (steadystate: SD: 0.62 °C), correspondingly. In addition, the forehead region has the highest skin temperature measurements among all identified regions (cooling: 33.55 ± 0.92 °C, heating: 33.02 ± 1.50 °C, steady-state: 33.77 ± 0.73 °C) while the ear region has the lowest measurements (cooling: 27.01 ± 1.36 °C, heating: 26.59 ± 1.47 °C, steady-state: 27.61 ± 1.51 °C). By examining column 2, 4, and 6, the skin temperature variations in the cooling (column 2) and heating (column 4) phases are much larger than those in the steady-state phase (column 6), which implies that facial skin temperature is affected by the ambient room temperature. On the other hand, the relatively small skin temperature deviations in the steady-state phase (column 6) suggest that the measurements are consistent when ambient room temperature is controlled at a constant level, which also indicates accurate measurements after applying the pre-processing approach discussed in Section 4.1. Moreover, nose and ear region have a larger temperature variation compared to other regions in the cooling (nose: 0.60 ± 0.25 °C, ear: 0.67 ± 0.20 °C) and heating phases (nose: 0.77 ± 0.34 °C, ear: 0.71 ± 0.43 °C). These two identified regions are potentially useful

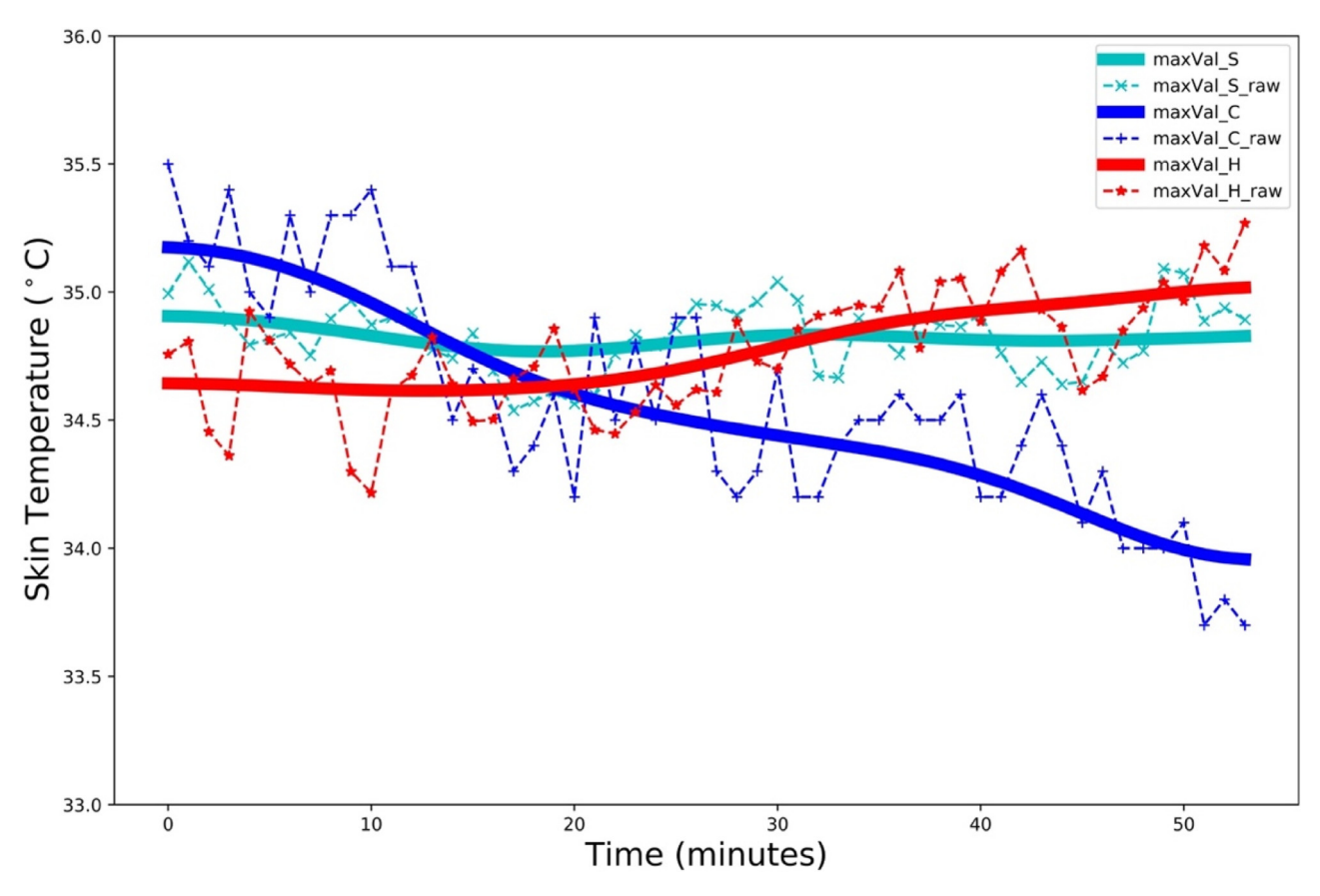


Fig. 9. Raw and processed maximum skin temperature of a subject in three phases (S: steady-state; C: cooling; H: heating).

Table 4 Statistics of skin temperature features in three phases.

Features	Cooling		Heating		Steady-State	
	$\bar{\mu} \pm SD(\bar{\mu})$ (1)	$\bar{s} \pm SD(\bar{s})$ (2)	$\bar{\mu} \pm SD(\bar{\mu})$ (3)	$\bar{s} \pm SD(\bar{s})$ (4)	$\bar{\mu} \pm SD(\bar{\mu})$ (5)	$\bar{s} \pm SD(\bar{s})$ (6)
maxVal ∇maxVal	34.38 ± 0.84 −0.016 ± 0.005	0.31 ± 0.11 0.013 ± 0.006	34.17 ± 0.93 0.004 ± 0.003	0.12 ± 0.04 0.009 ± 0.002	34.52 ± 0.62 −0.003 ± 0.003	0.08 ± 0.03 0.006 ± 0.003
forehead_avg forehead_max forehead_min ∇forehead	33.55 ± 0.92 34.17 ± 0.86 30.05 ± 0.72 -0.018 ± 0.007	0.34 ± 0.15 0.33 ± 0.13 0.44 ± 0.25 0.013 ± 0.005	33.02 ± 1.50 34.01 ± 1.08 29.58 ± 0.48 0.006 ± 0.009	0.19 ± 0.11 0.13 ± 0.05 0.20 ± 0.17 0.010 ± 0.002	33.77 ± 0.73 34.49 ± 0.62 30.16 ± 0.71 -0.002 ± 0.002	0.07 ± 0.02 0.09 ± 0.03 0.10 ± 0.09 0.006 ± 0.003
nose_avg nose_max nose_min ∇nose	32.46 ± 1.61 33.33 ± 1.20 30.87 ± 2.51 -0.032 ± 0.012	0.60 ± 0.25 0.45 ± 0.17 0.56 ± 0.20 0.022 ± 0.009	31.85 ± 0.66 32.80 ± 0.58 30.29 ± 1.50 0.032 ± 0.021	0.77 ± 0.34 0.46 ± 0.17 0.81 ± 0.33 0.034 ± 0.015	32.38 ± 1.54 33.21 ± 1.07 31.15 ± 2.05 -0.007 ± 0.007	0.22 ± 0.11 0.17 ± 0.09 0.20 ± 0.08 0.017 ± 0.012
cheek_avg cheek_max cheek_min ∇cheek	32.35 ± 1.84 33.62 ± 1.35 29.47 ± 2.40 -0.017 ± 0.006	0.35 ± 0.15 0.28 ± 0.15 0.53 ± 0.19 0.018 ± 0.005	31.86 ± 1.66 33.21 ± 1.16 29.05 ± 2.18 0.016 ± 0.006	0.31 ± 0.12 0.22 ± 0.08 0.56 ± 0.23 0.010 ± 0.002	32.70 ± 1.46 33.73 ± 1.12 30.32 ± 1.98 -0.001 ± 0.005	0.09 ± 0.05 0.10 ± 0.04 0.11 ± 0.05 0.007 ± 0.003
mouth_avg mouth_max mouth_min ∇mouth	33.42 ± 1.04 33.96 ± 0.95 32.75 ± 1.28 -0.016 ± 0.006	0.32 ± 0.13 0.28 ± 0.16 0.42 ± 0.16 0.019 ± 0.010	32.54 ± 1.10 33.43 ± 0.81 31.69 ± 1.39 0.004 ± 0.006	0.17 ± 0.05 0.15 ± 0.06 0.26 ± 0.13 0.015 ± 0.008	33.30 ± 0.90 33.88 ± 0.81 32.66 ± 1.10 0.000 ± 0.007	0.17 ± 0.06 0.12 ± 0.04 0.20 ± 0.08 0.013 ± 0.005
ear_avg ear_max ear_min ∇ear	27.01 ± 1.36 29.76 ± 1.81 25.30 ± 1.12 -0.035 ± 0.010	0.67 ± 0.20 0.62 ± 0.20 0.66 ± 0.25 0.032 ± 0.090	26.59 ± 1.47 29.21 ± 2.02 24.69 ± 1.21 0.039 ± 0.024	0.71 ± 0.43 0.70 ± 0.38 0.60 ± 0.46 0.021 ± 0.014	27.61 ± 1.51 30.35 ± 1.66 25.67 ± 1.39 0.003 ± 0.005	0.11 ± 0.05 0.19 ± 0.08 0.15 ± 0.10 0.010 ± 0.004
neck_avg neck_max neck_min ∇neck	32.75 ± 0.83 33.79 ± 0.61 29.78 ± 1.09 -0.014 ± 0.009	0.29 ± 0.18 0.30 ± 0.12 0.40 ± 0.29 0.018 ± 0.009	32.35 ± 0.96 33.55 ± 0.64 29.50 ± 1.11 0.011 ± 0.008	0.24 ± 0.11 0.14 ± 0.05 0.38 ± 0.31 0.010 ± 0.001	32.94 ± 0.92 33.90 ± 0.53 30.33 ± 1.28 0.000 ± 0.005	0.12 ± 0.06 0.07 ± 0.03 0.28 ± 0.21 0.011 ± 0.004

Note: all numbers are in °C.

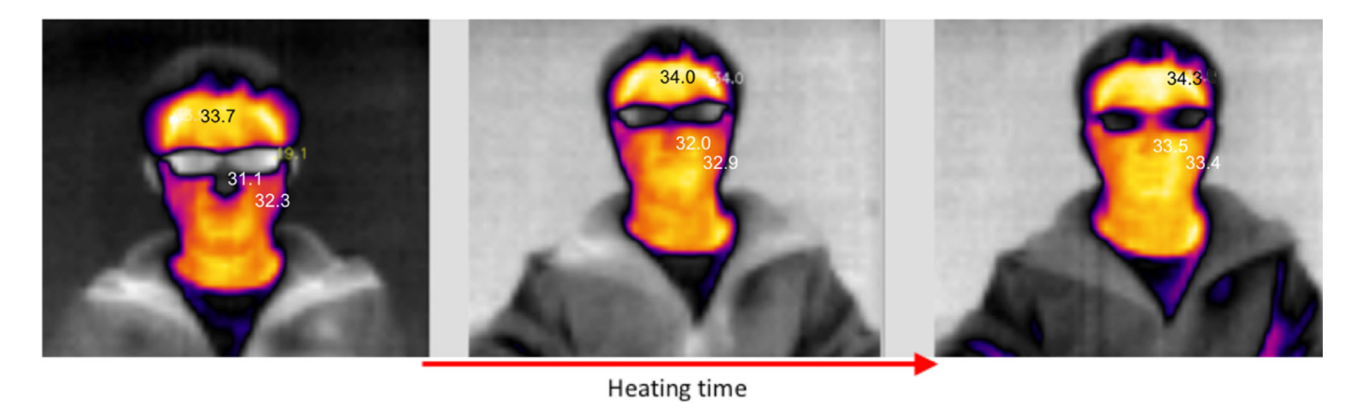


Fig. 10. Thermal images of the same subject in the heating phase at different time stamps (absolute temperature measurements are shown in the thermal images).

features to predict thermal preferences as they are more sensitive to the change of ambient environment. As an example, Fig. 10 shows three thermal images of the same subject captured at different time stamps in the heating phase. It is obvious that the nose region initially has a lower skin temperature which is shown in black (31.1 °C). This region gradually warms up (as shown in light red in the middle figure, 32.0 °C) and finally reaches its highest temperature (as shown in yellow in the right figure, 33.5 °C). It should be noted that the thermal images are generated based on normalized radiometric measurements to display a better temperature distribution in each frame. As a result, the colormap of thermal images is adjusted in real-time and the colors do not represent an absolute temperature scale. As shown in Fig. 10, while the face gradually warms up (the range of temperature increases), the glasses remain at an almost identical temperature and thus become darker over time (i.e., from grey to black).

In Table 4, all facial regions have negative mean temperature gradients in the cooling phase. On the other hand, all the mean temperature gradients are positive in the heating phase. These results are intuitive as during these two phases, human faces are constantly losing/gaining heat to/from the ambient environment. However, it is interesting to note that some facial regions (facial maxima, forehead, mouth) are more sensitive to cold stress than heat stress. For example, in the cooling phase the forehead region has a larger gradient than in the heating phase (|-0.018| > |0.006|) even though these two phases are kind of symmetric in terms of environment temperature (see Table 3). This finding implies that the significant features to predict thermal comfort may not remain the same under hot and cold stress and thus leads to different models based on the condition of the ambient environment.

To evaluate the relationship between different skin temperature features retrieved from the human face, Pearson correlation coefficients of all unique feature pairs in the three phases were calculated. Pearson correlation coefficient measures the strength and direction of the linear relationship between two variables (range between -1 and 1) where 1 represents perfect positive linear correlation and -1 represents perfect negative linear correlation and -1 represents perfect negative linear correlation coefficients of the 12 subjects in each particular phase of the experiment.

In the cooling phase (see Fig. 11), both intra-region (features extracted from a single facial region, e.g., mean, maxima and minima of the forehead) and inter-region features (features extracted from different facial regions, e.g., features in the forehead and cheeks) are highly correlated (minimum coefficient ρ = 0.74). This is due to the fact that different facial regions react in the same way under the cold stress and the corresponding skin temperature features are simultaneously decreasing over time.

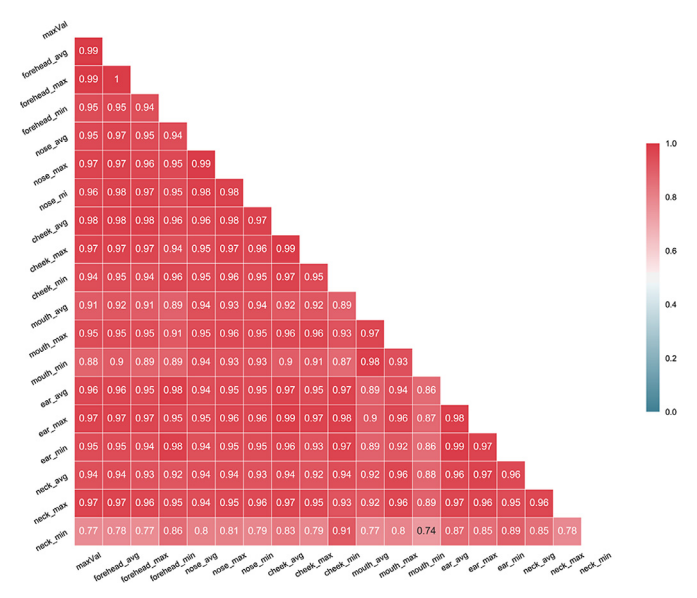


Fig. 11. Averaged Pearson correlation of different features in the cooling phase.

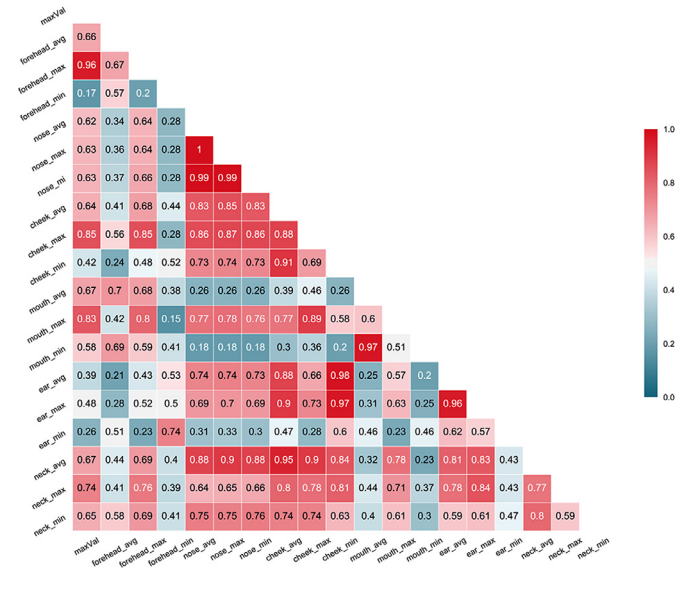


Fig. 12. Averaged Pearson correlation of different features in the heating phase.

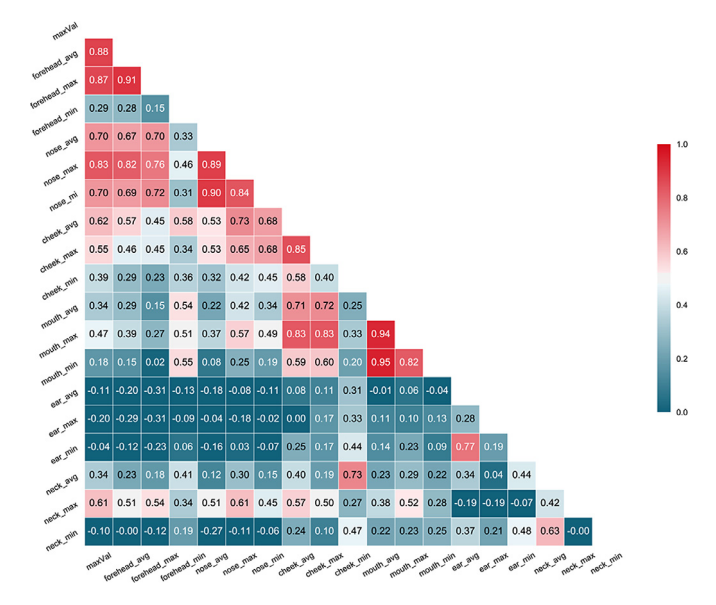


Fig. 13. Averaged Pearson correlation of different features in the steady-state phase.

However in the heating phase (see Fig. 12), it is important to note that only about one-third of features are highly correlated with a coefficient greater than 0.7. After checking the correlation coefficients of each subject, the authors found out that about onehalf of the subjects have the similar correlation coefficients as shown in the cooling phase while the other half have low correlations for some features, which indicates that personal variations in skin temperature responses exist in the heating phase. In the heating phase, the highly correlated features are mainly intraregion ones (e.g., the mean, maxima, minima of nose, cheeks, and ears) and inter-regions with larger variations or gradients in skin temperature (e.g., nose: 0.77 ± 0.34 °C; ears: 0.71 ± 0.43 °C; cheeks: 0.31 ± 0.12 °C, see Table 4). This result may be attributed to the lower sensitivity of certain facial regions (e.g., forehead) to the heat stress as discussed above. The skin temperature of these insensitive regions only varies in a limited range and may remain constant during a certain period of time in the heating phase, which leads to the low correlations.

For the steady-state phase (Fig. 13) where the room temperature is maintained relatively constant, only a few features are highly correlated (the pattern is also similar across several subjects). This is due to the same reason as discussed in the heating phase while in this case only the nose and mouth region show some temperature variations.

4.3. Thermal comfort prediction using the extracted features

In this paper, thermal comfort preference prediction can be translated into a classification problem where the subjects' preferences have three categorical values, i.e., warmer, cooler and neutral. Thus, the comfort prediction model is formulated as $TC = (T_{facial}, \nabla_{facial})$, where TC is the targeted variable thermal comfort. T_{facial} , ∇_{facial} are the skin temperature features extracted from each facial region and the corresponding gradients. Common machine learning methods including Support Vector Machine, Classification Tree, and Random Forest have been investigated to classify thermal comfort [[7],[8],[32–35]]. Among these existing methods, Chaudhuri et al. [[7],[8]], Li et al. [35], and Kim et al. [33] suggested that the Random Forest model produces better prediction results and provides useful interpretations (e.g., which feature is important).

Random Forest is an ensemble method which classifies an object by averaging a large collection of decision trees. This method applies bootstrap aggregating and can reduce the overfitting problem originated from decision trees [3]. As in this study, a total of 26 features (see Table 4) are considered for model training, Random Forest is an ideal method to randomly sample the training features at each split to reduce the variances in the training data. Also, it is worth noting that even though many features selected in this study are highly correlated (see Fig. 11–13), it does not affect the classification accuracy [27]. Correlated features generally reduce the interpretability of the model and are usually solved by feature extraction methods such as Principal Component Analysis. However, this is beyond the scope of this paper.

In this study, comfort prediction models were trained on each subject's dataset to develop personalized models. The Random Forest model was trained using the Python Scikit-learn package [40]. Hyper-parameters were tuned through the grid search to

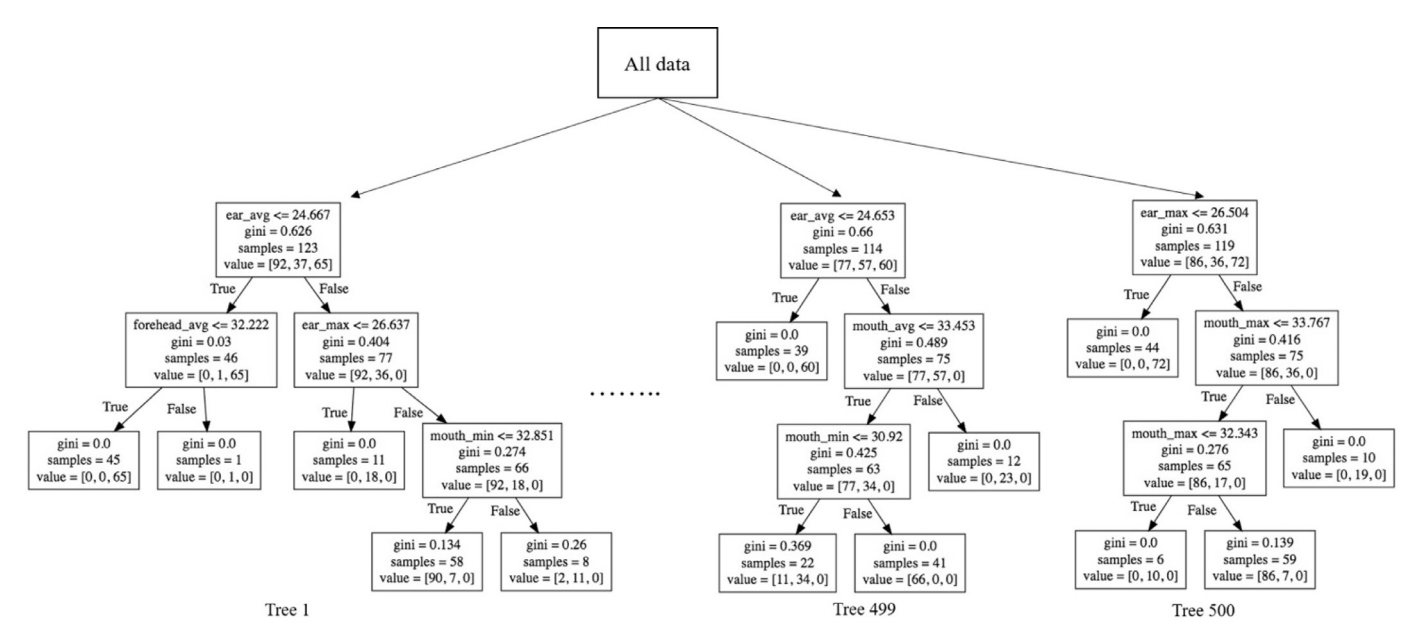


Fig. 14. Random Forest structure for a subject.

Table 5Prediction accuracy of the Random Forest model for each subject.

Subject ID	1	2	3	4	5	6	7	8	9	10	11	12	Avg.
Cooling Heating	0.935 0.916	0.825 0.840	0.875 0.932	0.921 0.946	0.935 0.955	0.947 0.955	0.921 0.942	0.946 0.933	0.942 0.933	0.921 0.952	0.943 0.942	0.882 0.873	0.916 0.927
General	0.730	0.801	0.829	0.921	0.900	0.878	0.859	0.854	0.830	0.885	0.906	0.812	0.850

exhaustively evaluate the accuracy of each configuration for performance optimization (i.e., 'n_estimators': [300, 500, 700, 1000], 'max_features': ['auto', 'sqrt', 'log2'], 'max_depth': [2, 3, 4, 5]). The maximum number of features allowed in the estimators and the maximum tree depth were intentionally controlled at a small size to reduce the problem of overfitting. Fig. 14 shows a Random Forest structure for a subject which consists of 500 classification trees. In this example, each tree is allowed to have a maximum depth of 3 and up to 5 features.

The optimal hyper-parameters for each subject's personalized comfort prediction model are shown in Appendix Table A.1. For each subject, three prediction models were evaluated, i.e., models for the cooling phase (denoted as "cooling" in Appendix Table A.1, which were developed using the data collected in the cooling phase); models for the heating phase (denoted as "heating", which were developed using the data collected in the heating phase); and general models (denoted as "general", which were developed using data from all three phases). Models for the steady-state phase were not developed separately as subjects' thermal preferences generally did not change throughout that phase.

After tuning the hyper-parameters, ten-fold cross validations were conducted to evaluate the prediction accuracy of comfort prediction models. The prediction accuracy of each subject's personalized comfort prediction model is shown in Table 5. On average, by using the selected facial skin temperature features, the personalized methods can achieve an 85.0% accuracy in predicting subjects' thermal comfort preferences and a slightly higher accuracy of 91.6% and 92.7% in the cooling and heating phases, respectively.

To identify the most significant features for thermal comfort prediction, the selected skin temperature features were ranked according to their contributions to reducing the loss function. The five most important features for each subject are presented in Appendix Table A.2. It can be seen that the significant features are subject-dependent. Also, these features are data-driven and may not remain identical as more data are collected in further experiments, e.g., in cooling seasons. However, features extracted from facial regions with a larger skin temperature variation such as ears, nose, and cheeks mostly appear to be the significant predictors, which indicates the ideal facial regions for future studies to analyze and interpret occupant's thermal preferences.

5. Discussion

The experimental results confirm that people's facial skin temperature varies with respect to the change of environment temperature. Due to the thermoregulatory control of human body, in general skin temperature tends to increase under the heat stress while decrease under the cold stress. In the heating phase, all the selected facial skin temperature features are highly correlated while for the cooling phase only about one third of these features still show a similar correlation. This finding indicates different sensitivities and response behaviors of the selected facial regions in the cooling and heating phases, which might be the effect of sweating under heat stress [39]. Another possible reason for this observation is that room temperature is not increased significantly in the heating phase (i.e., in excess of 30 °C) to observe large variations in some facial regions (e.g., forehead, nose).

In the experiments, the ambient room temperature is controlled to vary by about 5 °C (cooling phase: 27.5 - 22.6 °C; heating phase: 22.5 - 27.7 °C) as opposed to existing studies in which the room temperature variations can be as high as 10 °C [7,12,24]. Despite the relatively small changes in room temperature, statistically significant variations in skin temperature have been observed. Data from 12 subjects suggest that skin temperature of the selected facial regions react in different magnitudes, which may due to the different thickness of the subcutaneous fat layer, the density of blood vessels, and the amount of skin blood flow [41]. Under the cold stress, ears have the highest skin temperature variation, followed by the nose, cheeks, and forehead. Under the heat stress, the nose, ears, and cheeks tend to have larger temperature variations.

The significant regions for comfort prediction vary across subjects (Appendix Table A.2), which can be caused by personal variations that some subjects have a relatively stable overall or regional skin temperature than others. But in general, the susceptible facial regions to the change of environment temperature are proved to be the good predictors of thermal comfort in the Random Forest model. Except for a few cases (e.g., the general model for id9 and id11), the temperature gradients are not very helpful in the comfort interpretation. This is probably due to the fact that temperature gradient only implies how skin temperature changes but does not provide additional information about a subject's thermal comfort state. For example, a negative and substantial temperature gradient suggests that human body is losing heat to the ambient environment, however, this scenario can happen at any time during the cooling phase when the environment temperature is decreasing over time, which leads to a negative temperature gradient as observed in the data.

For the comfort prediction models, increasing the number of trees in the Random Forest by tuning 'n_estimators' does not always yield a better performance (as shown in Appendix Table A.1). In fact, there exists an optimal number of trees for each dataset such that a larger forest will make the prediction worse and also computationally expensive. This is probably because this model randomly samples features provided by the user in each tree. If the number of significant features is small compared to the nonsignificant ones, there is a higher chance that the model is built upon non-significant features (in other words, the noise) when the number of estimators becomes larger. For the maximum tree depth (i.e., the 'max_depth' parameter), a smaller depth (e.g., 2 or 3) is generally preferred as a deeper tree can cause the overfitting problem.

In terms of the prediction accuracy, as shown in Table 5, models solely trained on the cooling and heating dataset demonstrate a higher accuracy compared to the integrated dataset which consists of all three experiment phases. This can be attributed to the different thermal sensations under cooling, heating, and steady-state conditions even though the selected skin temperatures features are numerically close in different phases, which caused seemingly "contradictory". For example, when a subject's skin temperature increases to 34 °C under heat stress, he/she may have a different thermal sensation compared to the scenario when the skin temperature decreases to 34 °C under cold stress. In this case, the tem-

perature gradients might be a useful predictor because they help to differentiate the cold and heat stress.

It is also worth noting that the personalized prediction models only need to be trained once in the data collection experiment. Later, the pre-developed models can be applied to continuously predict each subject's comfort level in a non-intrusive manner. The potential applications of this non-intrusive comfort interpretation method can be adopted in a variety of thermal comfort related applications and contexts such as multi-occupancy offices, cars, trains where a promising approach to automatically and dynamically control the HVAC is much needed. During its usage, if more data are collected from the subjects (e.g., in different seasons), the prediction models can be updated using the newly received data to evolve over time.

However, this study also has some limitations. First, the experiments were only conducted in the heating seasons. The correlations of skin temperature features in the three phases (discussed in Section 4.2) and the performance of comfort prediction models (discussed in Section 4.3) may not hold for the cooling seasons. Thus, further investigations on different seasonal climates are still needed to evaluate the proposed approach. Second, some facial features may not always be visible to the camera in the operation. For example, during the experiment the authors found that fringes can interfere with the skin temperature measurement of the forehead region. In this case, the forehead region will have a lower measurement which may affect the result of predictions. Even worse, if the subject is blocked from the thermal camera, this method will not work due to the failure of data collection. Third, human factors such as clothing insulation and activity level were controlled and assumed constant in the experiments. However, in practice occupants' activity level or adaptive behaviors (e.g., put on a jacket, drink hot water) may affect their thermal sensations and preferences. Despite this framework being capable of capturing the thermoregulatory control of human body by monitoring the skin temperature, its performance in such situations still requires more detailed investigations. In this case, it can be helpful to incorporate additional human data from other data collection methods into the comfort prediction model, such as heart rate and activity level collected from a wristband as discussed in the authors' previous work [35]. Fourth, the impacts of glasses worn around the eyes on the measurement accuracy and facial skin temperature are unknown. For example, glasses may reflect the background temperature of the room, resulting in inaccurate measurements. As an additional layer, glasses may also affect the facial temperature in the heating and cooling processes. In this case, a comparative testing of subjects with and without glasses can be helpful to understand its impact. Fifth, despite the low-cost camera can achieve an acceptable accuracy through the pre-processing (Section 4.1), dynamic calibration of thermal camera (e.g., [37]) may further improve the prediction accuracy of thermal preference.

6. Conclusions

This paper presented a novel framework for real-time thermal comfort interpretation using infrared thermography. The main contribution of this paper is the proposed data collection and analysis framework to non-intrusively and automatically obtain, retrieve, and analyze facial skin temperature data and interpret thermal comfort conditions for each building occupant in real operational environments. The proposed framework leverages interdisciplinary techniques including the thermoregulatory theory, computer vision, and machine learning. Results demonstrate that facial skin temperature collected from non-intrusive low-cost infrared thermal cameras can help achieve a robust prediction of thermal comfort in real time, and offers the possibility for synchronous control of indoor environments with minimal interruption of building occupants. The resulting new knowledge from this study has the potential to transition the current building HVAC control from a passive and user-empirical process to an automated, user-centric and data-driven mechanism that can simultaneously improve occupant satisfaction and well-being in indoor environments.

The main conclusions from this study include: first, facial skin temperature is a useful bio-signal to analyze subjects' thermal comfort preferences. In the experiment, a variation of 5 °C in the room temperature shows statistically significant impacts on the facial skin temperature. Second, the data suggest that facial skin temperature is more sensitive to the cold stress than heat stress. A higher correlation between facial skin temperature features has been observed in the cooling experiments. Third, human ears, noses, and cheeks suggest a larger skin temperature variation. Features retrieved from these regions have been proven to be the most significant predictors for thermal comfort interpretation. Fourth, despite the low-cost thermal camera having a lower accuracy compared to the contact thermocouples or infrared thermometers adopted in other studies, by incorporating features collected from different facial regions, subjects' thermal comfort preference can be predicted with an 85% accuracy using the proposed framework

Acknowledgments

The authors would like to acknowledge the financial support for this research received from the U.S. National Science Foundation (NSF) CBET 1349921. Any opinions and findings in this paper are those of the authors and do not necessarily represent those of the NSF.

Appendix

Tables A.1 and A.2.

Table A.1Optimal hyper-parameters for each subject.

Subject ID	Cooling	Heating	General
1	n_estimators: 300max_depth: 2max_features: auto	n_estimators: 500max_depth: 2max_features: auto	n_estimators: 300max_depth: 2max_features: auto
2	n_estimators: 500max_depth: 2max_features: sqrt	n_estimators: 300max_depth: 2max_features: sqrt	• n_estimators: 1000 • max_depth: 2 • max_features: auto
3	n_estimators: 300max_depth: 4max_features: log2	n_estimators: 300max_depth: 2max_features: auto	n_estimators: 500max_depth: 2max_features: auto

(continued on next page)

Table A.1 (continued)

Subject ID	Cooling	Heating	General
4	n_estimators: 300max_depth: 2max_features: auto	n_estimators: 300max_depth: 2max_features: auto	• n_estimators: 1000 • max_depth: 3 • max_features: log2
5	n_estimators: 300max_depth: 2max_features: auto	n_estimators: 300max_depth: 2max_features: log2	n_estimators: 300max_depth: 3max_features: log2
6	n_estimators: 300max_depth: 2max_features: auto	n_estimators: 300max_depth: 2max_features: auto	n_estimators: 500max_depth: 3max_features: sqrt
7	n_estimators: 300max_depth: 2max_features: auto	n_estimators: 500max_depth: 2max_features: auto	n_estimators: 700max_depth: 2max_features: log2
8	n_estimators: 300max_depth: 2max_features: auto	n_estimators: 300max_depth: 2max_features: auto	n_estimators: 700max_depth: 5max_features: log2
9	n_estimators: 300max_depth: 2max_features: auto	n_estimators: 700max_depth: 2max_features: auto	n_estimators: 300max_depth: 5max_features: log2
10	n_estimators: 300max_depth: 2max_features: auto	• n_estimators: 300 • max_depth: 2 • max_features: auto	• n_estimators: 700 • max_depth: 3 • max_features: log2
11	n_estimators: 300max_depth: 2max_features: auto	n_estimators: 300max_depth: 2max_features: auto	• n_estimators: 700 • max_depth: 3 • max_features: sqrt
12	'n_estimators: 500max_depth: 3max_features: log2	'n_estimators: 500max_depth: 3max_features: log2	'n_estimators: 500max_depth: 3max_features: auto

Table A.2 Features importance of the Random Forest model for each subject.

Subject ID	Cooling	Heating	General
1	'ear_avg''ear_max''nose_avg''forehead_min''ear_min'	'ear_max''cheek_max''nose_avg''forehead_avg''cheek_min'	'cheek_min''nose_avg''nose_max''ear_max''ear_avg'
2	'forehead_min''forehead_avg''nose_min''neck_max''cheek_max'	'ear_max''mouth_min''cheek_max''neck_min''mouth_avg'	'cheek_max''cheek_avg''ear_max''forehead_min''nose_max'
3	'cheek_max''ear_max''nose_min''nose_max''nose_avg'	'Vforehead''ear_max''cheek_max''ear_avg''nose_min'	'ear_avg''ear_min''ear_max''forehead_avg''neck_avg'
4	'mouth_min''mouth_avg''cheek_max''ear_max''nose_avg'	'ear_max''cheek_max''neck_min''cheek_avg''ear_avg'	'ear_max''cheek_min''forehead_min''ear_min''ear_avg'
5	'ear_max''nose_min''forehead_min''nose_avg''mouth_avg'	· 'cheek_max' · 'ear_max' · 'nose_avg' · 'nose_max' · 'neck_avg'	'maxVal''forehead_avg''forehead_max''cheek_min''neck_avg'
6	'ear_max''cheek_max''nose_max''mouth_avg''mouth_min'	'ear_max''nose_avg''cheek_avg''ear_avg''nose_max'	'ear_avg''ear_max''cheek_avg''cheek_max''mouth_max'

(continued on next page)

Table A.2 (continued)

Subject ID	Cooling	Heating	General
7	'nose_avg''nose_min''ear_min''forehead_min''mouth_avg'	'ear_max''nose_avg''nose_max''ear_avg''cheek_min'	'ear_max''mouth_avg''forehead_avg''mouth_min''neck_avg'
8	'nose_max''nose_avg''forehead_min''forehead_avg''ear_avg'	'cheek_max''neck_min''ear_avg''ear_min''neck_max'	'nose_avg''ear_avg''neck_max''nose_min''ear_min'
9	 'forehead_min' 'forehead_avg' '∇neck' 'maxVal' 'neck_max' 	'ear_max''∇neck''forehead_avg''cheek_avg''ear_avg'	'nose_max''nose_min''nose_avg''forehead_min''∇neck'
10	'cheek_max''mouth_min''ear_max''nose_min''nose_avg'	• 'ear_avg' • 'cheek_min' • 'ear_min' • '∇ear' • 'mouth_min'	'mouth_max''nose_max''mouth_avg''mouth_min''cheek_max'
11	 'forehead_min' 'nose_max' '∇ear' 'forehead_avg' 'maxVal' 	'cheek_max''ear_max''nose_avg''neck_min''mouth_avg'	'nose_max''forehead_avg''neck_max''forehead_min''∇ear'
12	'nose_avg''cheek_avg''forehead_avg''ear_max''cheek_min'	'ear_avg'forehead_avg''ear_max''mouth_avg''forehead_max'	'nose_avg''forehead_avg''nose_max''ear_avg''cheek_avg'

References

- [1] M. Abouelenien, M. Burzo, R. Mihalcea, Human acute stress detection via integration of physiological signals and thermal imaging, in: Proceedings of the 9th ACM International Conference on PErvasive Technologies Related to Assistive Environments, ACM, 2016, p. 32.
- [2] ASHRAE Standard, Standard 55-2010: "Thermal Environmental Conditions For Human Occupancy", ASHRAE, Atlanta USA, 2010.
- [3] L. Breiman, Random forests, Mach. Learn. 45 (1) (2001) 5-32.
- [4] G.S. Brager, R. de Dear, A standard for natural ventilation, ASHRAE J 42 (10)
- [5] M. Burzo, M. Abouelenien, V. Perez-Rosas, C. Wicaksono, Y. Tao, R. Mihalcea, Using infrared thermography and biosensors to detect thermal discomfort in a buildings inhabitants, in: Proceedings of the ASME 2014 International Mechanical Engineering Congress and Exposition, American Society of Mechanical Engineers, 2014, pp. 1–11.
- [6] M. Burzo, C. Wicaksono, M. Abouelenien, V.P. erez Rosas, R. Mihalcea, and Y. Tao (2014). Multimodal sensing of thermal discomfort for adaptive energy saving in buildings. In iiSBE Net Zero Built Environment 2014 Symposium.
- [7] T. Chaudhuri, D. Zhai, Y.C. Soh, H. Li, L. Xie, Thermal comfort prediction using normalized skin temperature in a uniform built environment, Energy Build. 159 (2018) 426–440.
- [8] T. Chaudhuri, D. Zhai, Y.C. Soh, H. Li, L. Xie, Random forest based thermal comfort prediction from gender-specific physiological parameters using wearable sensing technology, Energy Build. 166 (2018) 391–406.
- [9] N. Charkoudian, Skin blood flow in adult human thermoregulation: how it works, when it does not, and why, in: Proceedings of the Mayo Clinic Proceedings, 78, Elsevier, 2003, pp. 603–612. Vol., No.
- [10] C.P. Chen, R.L. Hwang, S.Y. Chang, Y.T. Lu, Effects of temperature steps on human skin physiology and thermal sensation response, Build. Environ. 46 (11) (2011) 2387–2397.
- [11] J.H. Choi, D. Yeom, Study of data-driven thermal sensation prediction model as a function of local body skin temperatures in a built environment, Build. Environ. 121 (2017) 130–147.
- [12] J.H. Choi, V. Loftness, Investigation of human body skin temperatures as a bio-signal to indicate overall thermal sensations, Build. Environ. 58 (2012) 258–269
- [13] R. de Dear, Recent enhancements to the adaptive comfort standard in ASHRAE 55-2010, in: Proceedings of the 45th Annual Conference of the Architectural Science Association, Sydney, Australia, 2011.
- [14] R.J. de Dear, G.S. Brager, Thermal comfort in naturally ventilated buildings: revisions to ASHRAE Standard 55, Energy Build. 34 (6) (2002) 549–561.

- [15] F. De Oliveira, S. Moreau, C. Gehin, A. Dittmar, Infrared imaging analysis for thermal comfort assessment, in: Proceedings of the Engineering in Medicine and Biology Society, 2007. EMBS 2007. 29th Annual International Conference of the IEEE, IEEE, 2007, pp. 3373–3376.
- [16] Department of Energy (DOE), Heating & Cooling, 2017. Accessed on June 15from https://energy.gov/public-services/homes/heating-cooling.
- [17] V.L. Erickson, A.E. Cerpa, Thermovote: participatory sensing for efficient building hvac conditioning, in: Proceedings of the Fourth ACM Workshop on Embedded Sensing Systems for Energy-Efficiency in Buildings, ACM, 2012, pp. 9–16.
- [18] European Commission, 2016. An EU Strategy on Heating and Cooling. Accessed on October 1, 2017, from https://ec.europa.eu/energy/sites/ener/files/documents/1_EN_ACT_part1_v14.pdf.
- [19] P.O. Fanger, Thermal Comfort: Analysis and Applications in Environmental Engineering, McGraw-Hill, Berkeley, CA, 1970.
- [20] M. Feldmeier, J.A. Paradiso, Personalized HVAC control system, in: Proceedings of the Internet of Things (IOT), 2010, IEEE, 2010, pp. 1–8.
- [21] FLIR Lepton with Radiometry Datasheet, 2014.
- [22] FLIR 5 Factors influencing radiometric temperature measurements, 2016. Retrieved from http://www.cvl.isy.liu.se/education/undergraduate/tsbb09/lectures/Guidebook_Cores_5_Factors_Influencing_Radiometric_Temperature_Measurements.pdf.
- [23] M. Frontczak, S. Schiavon, J. Goins, E. Arens, H. Zhang, P. Wargocki, Quantitative relationships between occupant satisfaction and satisfaction aspects of indoor environmental quality and building design, Indoor Air 22 (2) (2012) 119–131.
- [24] A. Ghahramani, G. Castro, B. Beccrik-Gerber, X. Yu, Infrared thermography of human face for monitoring thermoregulation performance and estimating personal thermal comfort, Build. Environ. 109 (2016) 1–11.
- [25] L.A. Hang-yat, D. Wang, Carrying my environment with me: A participatory-sensing approach to enhance thermal comfort, in: Proceedings of the 5th ACM Workshop on Embedded Systems For Energy-Efficient Buildings, ACM, 2013, pp. 1–8.
- [26] M. Humphreys, F. Nicol, S. Roaf, O. Sykes, Standards For Thermal comfort: Indoor Air Temperature Standards For the 21st Century, Routledge, 2015.
- [27] G. James, D. Witten, T. Hastie, R. Tibshirani, An Introduction to Statistical Learning, 112, springer, New York, 2013.
- [28] F. Jazizadeh, A. Ghahramani, B. Becerik-Gerber, T. Kichkaylo, M. Orosz, Human-building interaction framework for personalized thermal comfort-driven systems in office buildings, J. Comput. Civil Eng. 28 (1) (2013) 2–16.
- [29] W. Jung, F. Jazizadeh, Non-Intrusive detection of respiration for smart control of HVAC system, in: Proceedings of teh Computing in Civil Engineering 2017, 2017, pp. 310–317.

- [30] S. Karjalainen, Gender differences in thermal comfort and use of thermostats in everyday thermal environments. Build, Environ, 42 (4) (2007) 1594–1603.
- [31] C. Karmann, S. Schiavon, E. Arens, Percentage of commercial buildings showing at least 80% occupant satisfied with their thermal comfort, in: Proceedings of the Windsor Conference, 2018, pp. 1–7.
- [32] J. Kim, S. Schiavon, G. Brager, Personal comfort models—A new paradigm in thermal comfort for occupant-centric environmental control, Build. Environ. (2018).
- [33] J. Kim, Y. Zhou, S. Schiavon, P. Raftery, G. Brager, Personal comfort models: predicting individuals' thermal preference using occupant heating and cooling behavior and machine learning, Build. Environ. 129 (2018) 96–106.
- [34] D. Li, C.C. Menassa, V.R. Kamat, A personalized HVAC control smartphone application framework for improved human health and well-being, in: Proceedings of the Computing in Civil Engineering, 2017, pp. 82–90.
- [35] D. Li, C.C. Menassa, V.R. Kamat, Personalized human comfort in indoor building environments under diverse conditioning modes, Build. Environ. 126 (2017) 304–317.
- [36] S. Liu, M. Jin, H. Das, C. Spanos, S. Schiavon, Personal thermal comfort models based on physiological parameters measured by wearable sensors, in: Proceedings of the Windsor Conference, 2018, pp. 431–441.
- [37] H. Metzmacher, D. Wölki, C. Schmidt, J. Frisch, C. van Treeck, Real-time human skin temperature analysis using thermal image recognition for thermal comfort assessment, Energy Build. 158 (2018) 1063–1078.
- [38] A.Y. Owda, N. Salmon, S.W. Harmer, S. Shylo, N.J. Bowring, N.D. Rezgui, M. Shah, Millimeter-wave emissivity as a metric for the non-contact diagnosis of human skin conditions, Bioelectromagnetics 38 (7) (2017) 559–569.
- [39] K. Parsons, Human thermal environments: the effects of hot, moderate, and cold environments on human health, comfort, and performance, CRC Press, 2014.
- [40] F. Pedregosa, G. Varoquaux, A. Gramfort, V. Michel, B. Thirion, O. Grisel, J. Vanderplas, Scikit-learn: machine learning in python, J. Mach. Learn. Res 12 (Oct) (2011) 2825–2830.
- [41] P.M. Prendergast, Anatomy of the face and neck, in: Cosmetic Surgery, Springer, Berlin Heidelberg, 2013, pp. 29–45.
- [42] S. Purdon, B. Kusy, R. Jurdak, G. Challen, Model-free HVAC control using occupant feedback, in: Proceedings of the, 2013 IEEE 38th Conference on Local Computer Networks Workshops (LCN Workshops), IEEE, 2013, pp. 84–92.

- [43] J. Ranjan, J. Scott, ThermalSense: determining dynamic thermal comfort preferences using thermographic imaging, in: Proceedings of the 2016 ACM International Joint Conference on Pervasive and Ubiquitous Computing, ACM, 2016, pp. 1212–1222.
- [44] C.A. Roulet, N. Johner, F. Foradini, P. Bluyssen, C. Cox, E. de Oliveira Fernandes, C. Aizlewood, Perceived health and comfort in relation to energy use and building characteristics, Build. Res. Inf. 34 (5) (2006) 467–474.
- [45] M. Schweiker, A. Wagner, A framework for an adaptive thermal heat balance model (ATHB), Build. Environ. 94 (2015) 252–262.
- [46] Sparkfun MLX90614 IR Thermometer Hookup Guide, 2016. Retrieved from https://learn.sparkfun.com/tutorials/mlx90614-ir-thermometer-hookup-guide? ga=2.30906743.973887521.1521512244-603345122.1518317929.
- [47] SPSS: Pearson Correlation, 2018. Retrieved from https://libguides.library.kent. edu/SPSS/PearsonCorr.
- [48] G.I. Taylor, in: The Blood Supply of the Skin, Grabb and Smith's Plastic Surgery, fifth ed., Lippincott-Raven, Philadelphia, 1997, pp. 47–59.
- [49] P. Viola, M. Jones, Rapid object detection using a boosted cascade of simple features, in: Proceedings of the 2001 IEEE Computer Society Conference on Computer Vision and Pattern Recognition, 2001. CVPR 2001, IEEE, 2001 Vol. 1, pp. 1-1.
- [50] WELL Building Standard, 2014. Retrieved from https://www.wellcertified. com/sites/default/files/resources/WELL%20Building%20Standard%20-%20Oct% 202014.pdf.
- [51] T. Witterseh, D.P. Wyon, G. Clausen, The effects of moderate heat stress and open-plan office noise distraction on SBS symptoms and on the performance of office work, Indoor Air 14 (s8) (2004) 30–40.
- [52] R. Yao, B. Li, J. Liu, A theoretical adaptive model of thermal comfort-Adaptive predicted mean vote (aPMV), Build. Environ. 44.10 (2009) 2089–2096.
- [53] Y. Yao, Z. Lian, W. Liu, Q. Shen, Experimental study on skin temperature and thermal comfort of the human body in a recumbent posture under uniform thermal environments, Indoor Built Environ. 16 (6) (2007) 505–518.
- [54] B. Yi, J.H. Choi, Facial skin temperature as a proactive variable in a building thermal comfort control system, in: Proceedings of the Sustainable Human-Building Ecosystems, 2015, pp. 117–125.
- [55] H. Zhang, E. Arens, C. Huizenga, T. Han, Thermal sensation and comfort models for non-uniform and transient environments: Part I: Local sensation of individual body parts, Build. Environ. 45 (2) (2010) 380–388.